CRS-stack-based seismic imaging for rough top-surface topography

Z. Heilmann and M. von Steht

email: *Zeno.Heilmann@gpi.uni-karlsruhe.de*

keywords: *CRS-stack-based-imaging, kinematic wavefield attributes, surface topography, residual static corrections, tomographic inversion, depth migration*

ABSTRACT

In the current situation of rapidly growing demand in oil and gas, on-shore exploration, even under difficult conditions, becomes again more and more important. Unfortunately, rough top-surface topography and a strongly varying weathering layer often result in poor data quality which makes conventional data processing very difficult to apply. In recent years, many case studies demonstrated that the Common-Reflection-Surface (CRS) stack produces reliable stack sections with high resolution and superior signal-to-noise ratio compared to conventional methods. In order to define optimal spatial stacking operators, the CRS stack extracts for every sample of the zero-offset (ZO) section an entire set of physically interpretable stacking parameters, so-called kinematic wavefield attributes. As will be shown, these CRS attributes, obtained as a by-product of the data-driven stacking process, may be even more important than the stacked section itself. They can be applied to solve various dynamic and kinematic stacking, modeling, and inversion problems. CRS-stack-based seismic imaging makes use of these extended possibilities during the stack and in further processing.

The presented extention of the CRS-stack-based imaging workflow provides support for arbitrary top-surface topography. Its implementation combines two different approaches of topography handling to a cascaded processing strategy demanding very little additional effort. Finally, the CRS stack and also CRS-stack-based residual static corrections can be applied to the original prestack data without the need of any elevation statics. By a redatuming procedure, the CRS-stacked ZO section, the kinematic wavefield attribute sections, and the quality control sections can be related to a chosen planar measurement level. Thus, an ideal input for a preliminary interpretation and subsequent CRS-stack-based processing steps is provided.

INTRODUCTION

Obtaining a sufficiently accurate image, either in time or in depth domain, is often a difficult task in regions governed by complex geological structure and/or complicated near-surface conditions. Under such circumstances where simple model assumptions may fail it is of particular importance to extract as much information as possible directly from the measured data. Fortunately, the ongoing increase in available computing power makes so-called data-driven approaches (e. g., Hubral, 1999) feasible which, thus, have increasingly gained in relevance, during the last years.

The Common-Reflection-Surface (CRS) stack (e. g., Müller, 1999; Jäger et al., 2001; Mann, 2002) is one of these promising methods. Besides an improved zero-offset (ZO) simulation, its decisive advantage over conventional methods is that several so-called kinematic wavefield attributes are obtained as a by-product of the data-driven stacking process. As will be shown, they can be applied both to improve the stack itself and to support subsequent processing steps as, e.g., tomographic inversion or depth migration. With these *CRS attributes* an advanced data-processing workflow can be established leading from time to depth domain, covering a broad range of seismic reflection imaging issues in a consistent manner. The major steps of this workflow are displayed in Figure 1.

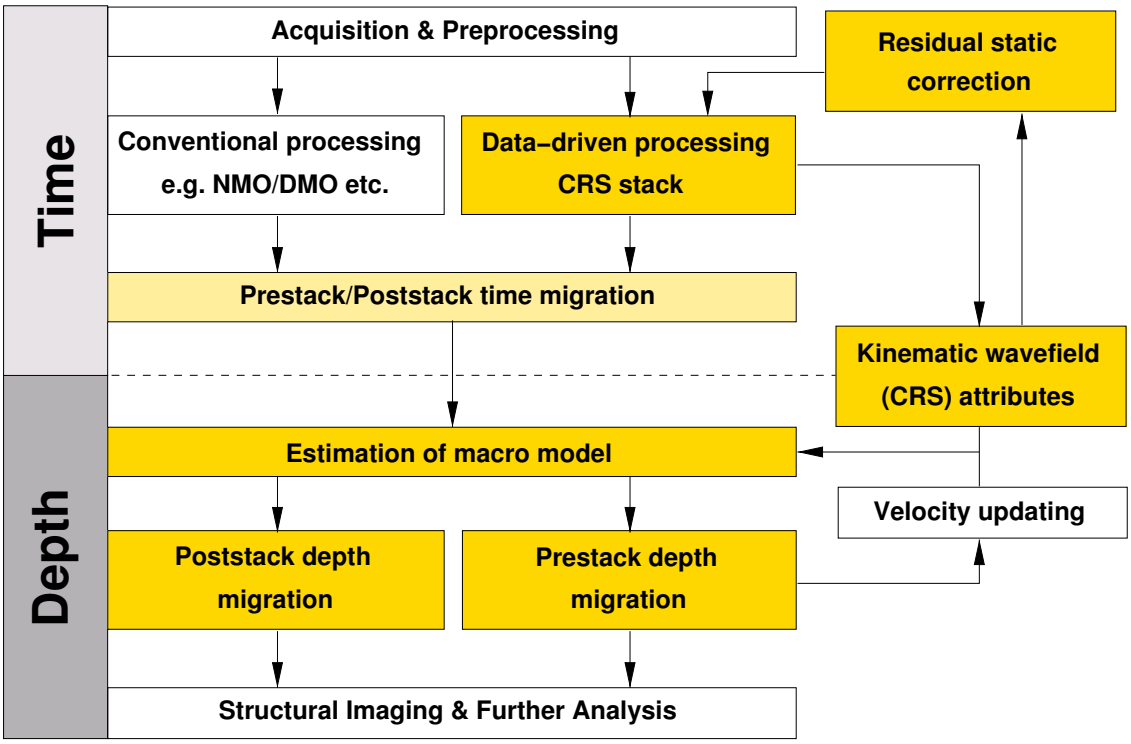

Figure 1: Major steps of seismic reflection data processing in time and depth domain. CRS-stack-based imaging procedures are highlighted yellow.

So far, this workflow was limited to data acquired on a planar measurement surface or at least to data for which a planar measurement surface had been simulated by elevation statics. However, conventional elevation statics may introduce a certain error to the stack and—even worse—to the CRS attribute sections, as a vertical emergence of all rays has to be assumed. In case of rough top-surface topography this can significantly deteriorate the results of the CRS stack and of all succeeding processing steps. This paper focuses on a sophisticated integration of topography handling into this CRS-stack-based imaging workflow. For this purpose it was necessary to solve two main issues:

1. To extent the CRS stack software to consider not only the lateral position of sources and receivers, but also their elevation.

2. To implement a redatuming procedure which transfers the CRS stack results from a floating datum that corresponds to the smoothed measurement surface to a constant reference datum corresponding to a fictitious planar measurement surface.

In recent years two different CRS stacking operators that consider the top-surface topography have been developed at Karlsruhe University. Chira et al. (2001) and Heilmann (2003) assume a smoothly curved measurement surface where all source and receiver locations contributing to a single stacking process can be approximated by a parabola. In Zhang (2003) a very general CRS stacking operator was presented that directly considers the true elevation of every source and receiver. The first approach is attractive from the computational point of view as it is possible to adopt most parts of the conventional CRS stack implementation. Especially, the pragmatic CRS-attribute search strategy using three one-parameter searches to determine the optimal stacking operator can be maintained. However, small elevation statics are still required in order to transfer the real data to the chosen smoothly curved measurement surface. The second approach demands far more computational effort, as two of the three attributes have to be searched for simultaneously due to the higher complexity of the stacking operator. On the other hand, no elevation statics are required and the z-coordinate of the emergence points of the simulated ZO rays can be chosen arbitrarily. Promissing results of this approach were presented in Zhang and Wu (2004).

REVIEW: CRS STACK CONSIDERING THE MEASUREMENT SURFACE TOPOGRAPHY.

Based on the ray-theoretical foundations presented in Červený (2001), Zhang derived a very general CRS stacking operator for arbitrary top-surface topography (see, e.g., Zhang, 2003). This stacking operator describes the second order traveltime moveout of any ray in the paraxial vicinity of a chosen *central ray* by means of physically interpretable properties. These properties, called kinematic wavefield attributes, are directly related to the central ray. For comparison, in case of the well known common-midpoint (CMP) stack we have only one kinematic wavefield attribute, i.e., the normal-moveout (NMO) velocity. For the specific geometry of CMP experiments on a planar measurement surface this single parameter is sufficient to describe the traveltime moveout with offset up to the second order. In contrast to this, the CRS stack operator also takes neighboring CMP experiments into account, i.e., describes the traveltime moveout with offset and midpoint dislocation.

In case of the ZO CRS stack, we choose the central ray to have the coincident source and receiver location X_0. If we denote the traveltime of paraxial rays by t and the traveltime of the central ray by t_0, the (hyperbolic) CRS stacking operator for arbitrary topography reads

$$\begin{aligned} t^2_{\mathrm{hyp}}(\Delta\vec{\mathsf{m}},\vec{\mathsf{h}})^{\mathrm{ZO}} &= \left(t_0 - \frac{2}{v_0}\,\left(\Delta m_x \sin\beta_0 + \Delta m_z \cos\beta_0\right)\right)^2 \\ &+ \frac{2\,t_0\,K_{\mathrm{N}}}{v_0}\,\left(\Delta m_x \cos\beta_0 - \Delta m_z \sin\beta_0\right)^2 \\ &+ \frac{2\,t_0\,K_{\mathrm{NIP}}}{v_0}\,\left(h_x \cos\beta_0 - h_z \sin\beta_0\right)^2\,, \end{aligned} \tag{1}$$

where $(\Delta m_x, \Delta m_z)$ and (h_x, h_z) are the components of midpoint displacement $\Delta\vec{\mathsf{m}} = \vec{\mathsf{m}} - \vec{\mathsf{m}}_{X_0}$ and half-offset $\vec{\mathsf{h}}$ of the considered paraxial ray according to Figure 2. The searched for CRS attributes are β_0, i.e., the emergence angle of the central ray in X_0, as well as K_{N} and K_{NIP}, two wavefront curvatures related to hypothetical experiments firstly introduced by Hubral (1983). The parameter v_0 defines the near-surface velocity and is assumed to be known a priori.

This traveltime approximation simplifies considerably if we assume a smoothly curved measurement surface that can be described locally by a parabola with apex in X_0. For this purpose, we establish a local Cartesian coordinate system as depicted in Figure 2, with its origin in X_0 and its x-axis being tangent to the surface in X_0. Here, the surface elevation z in the vicinity of X_0, expressed as a function of the horizontal displacement x, can be written as

$$z(x) = \frac{K_0}{2}x^2\,, \quad \text{with} \quad K_0 = \left.\frac{d^2z}{dx^2}\right|_{x_0} \tag{2}$$

being the local curvature of the measurement surface in X_0. Figure 2 shows a convex section of the smoothed measurement surface. By means of equation (2) the local Cartesian coordinates x, z of two points S and G located on the smoothed measurement surface can be written as

$$\begin{pmatrix} x(S) \\ z(S) \end{pmatrix} = \begin{pmatrix} m_x - h_x \\ -\frac{K_0}{2}(m_x - h_x)^2 \end{pmatrix} \qquad \text{and} \qquad \begin{pmatrix} x(G) \\ z(G) \end{pmatrix} = \begin{pmatrix} m_x + h_x \\ -\frac{K_0}{2}(m_x + h_x)^2 \end{pmatrix}. \tag{3}$$

Restating the expression for the midpoint vector by using equations (3) leads to

$$\vec{\mathsf{m}}(S,G) = \begin{pmatrix} m_x \\ m_z \end{pmatrix} = \frac{1}{2}\begin{pmatrix} x(G) + x(S) \\ z(G) + z(S) \end{pmatrix} = \begin{pmatrix} m_x \\ -\frac{K_0}{2}(m_x^2 + h_x^2) \end{pmatrix}. \tag{4}$$

In this way, a first order instance for m_z turns out to be a second order instance in terms of m_x and h_x. Due to the fact that we are looking for a second-order traveltime approximation and no first order term of h_z occurs in equation (1), it is not necessary to rewrite h_z in terms of m_x and h_x. At first glance, it might appear strange that the representation of m_z in equation (4) consists of two terms and depends not only on m_x but also on h_x. The explanation is given in Figure 2. The first term of m_z accounts for the

z-component of $\vec{\mathfrak{m}}^\star$. The second term represents the difference between $\vec{\mathfrak{m}}^\star$ and $\vec{\mathfrak{m}}$. Since we use for every X_0 a local Cartesian coordinate system with origin in X_0, $\Delta\vec{\mathfrak{m}}$ is equal $\vec{\mathfrak{m}}$ and $\vec{\mathfrak{m}}_{X_0}$ becomes zero. By replacing the first-order occurrence of m_z in equation (1) and by neglecting all higher-order terms of m_z and h_z we obtain

$$\begin{aligned} t^2_{\mathrm{hyp}}(m_x, h_x) &= \left(t_0 + \frac{2}{v_0}\, m_x\, \sin\beta_0\right)^2 \\ &+ \frac{2\, t_0}{v_0}\, \left(K_{\mathrm{N}}\, \cos^2\beta_0 - K_0\, \cos\beta_0\right)\, m_x^2 \\ &+ \frac{2\, t_0}{v_0}\, \left(K_{\mathrm{NIP}}\, \cos^2\beta_0 - K_0\, \cos\beta_0\right)\, h_x^2 \,. \end{aligned} \tag{5}$$

Using a local Cartesian coordinate system is a convenient choice for the derivation of equation (5). However, for the final implementation a global coordinate system is better suited, as this allows to use the same coordinate system for every X_0. For this purpose, we have to apply a coordinate transformation consisting of:

- a translation of the coordinate system, relating every local coordinate system to the same global origin and
- a rotation of the coordinate system by the local dip α_0, making the z-axis always point in depth direction [see Figure (3)].

This leads to the transformations

$$m_x = \frac{1}{\cos\alpha_0}\,(m_g - m_{g_0}) = \frac{1}{\cos\alpha_0}\,\Delta m_g \qquad \text{and} \qquad h_x = \frac{1}{\cos\alpha_0}\, h_g\,, \tag{6}$$

with m_{g_0} indicating the x-coordinate of X_0 in the global coordinate system. In contrast to formula (5), where the dip α_0 was implicitly comprised by the local coordinate system, in global coordinates one has to explicitly consider α_0 in the traveltime expressions. The emergence angle β_0, related to the surface normal in X_0 has to be transfered to β_0^g which is related to the depth direction [see Figure (3)]. Doing this yields the CRS traveltime operator in global coordinates:

$$\begin{aligned} t^2_{\mathrm{hyp}}(\Delta m_g, h_g) &= \left(t_0 + \frac{2\,\Delta m_g}{v_0\, \cos\alpha_0}\, \sin(\beta_0^g - \alpha_0)\right)^2 \\ &+ \frac{2\, t_0\, \Delta m_g^2}{v_0\, \cos^2\alpha_0}\, \left(K_{\mathrm{N}}\, \cos^2(\beta_0^g - \alpha_0) - K_0\, \cos(\beta_0^g - \alpha_0)\right) \\ &+ \frac{2\, t_0\, h_g^2}{v_0\, \cos^2\alpha_0}\, \left(K_{\mathrm{NIP}}\, \cos^2(\beta_0^g - \alpha_0) - K_0\, \cos(\beta_0^g - \alpha_0)\right)\,. \end{aligned} \tag{7}$$

Setting $K_0 = 0$ and $\alpha_0 = 0$ this traveltime operator reduces to the standard ZO CRS stack formula for a planar measurement surface (see, e.g. Höcht, 1998; Müller, 1999; Mann, 2002). For convenience this formula (in different notation) is repeated here. It reads

$$\begin{aligned} t^2_{\mathrm{hyp,planar}}(\Delta m, h) &= \left(t_0 + \frac{2}{v_0}\, \Delta m\, \sin\beta_0\right)^2 \\ &+ \frac{2\, t_0}{v_0}\, K_{\mathrm{N}}\, \cos^2\beta_0\, \Delta m^2 \\ &+ \frac{2\, t_0}{v_0}\, K_{\mathrm{NIP}}\, \cos^2\beta_0\, h^2\,, \end{aligned} \tag{8}$$

with $\beta_0 = \beta_0^g$, $\Delta m = \Delta m_g$, and $h = h_g$.

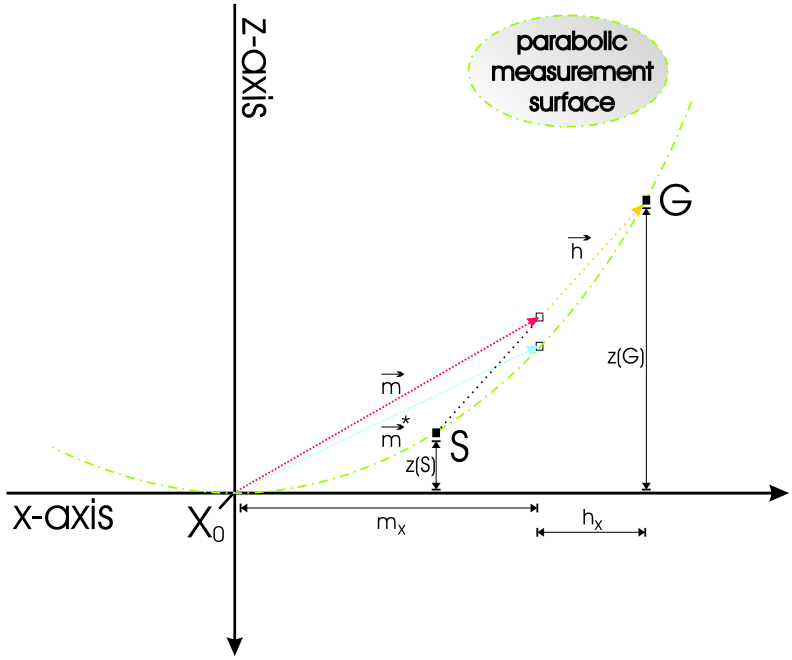

Figure 2: *Sketch of a parabolic section of a smoothed measurement surface. The vector $\vec{m}^*$ points to that point on the surface which is defined by the x-coordinate of the midpoint vector $\vec{m}$ (Figure according to von Steht, 2004).*

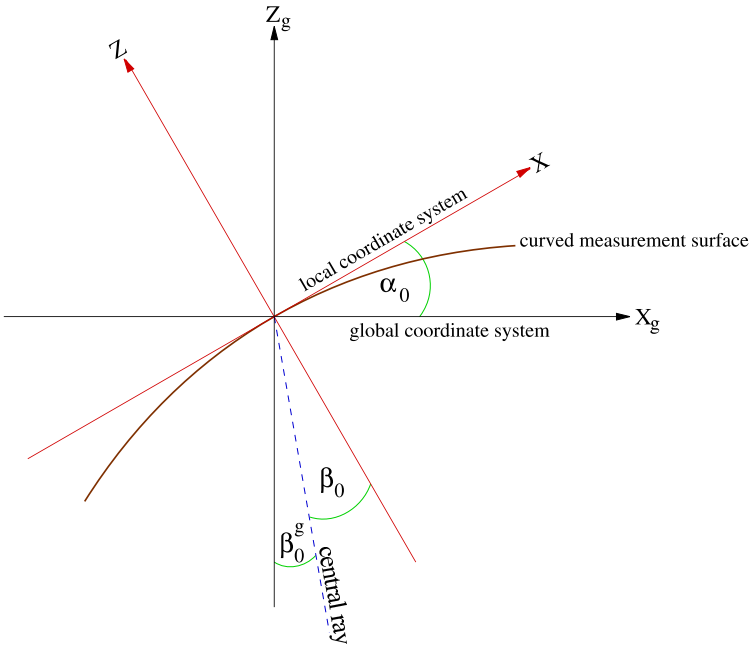

Figure 3: *The relationship between the emergence angles β_0, β_0^g, and the dip angle α_0 for a curved measurement surface. Note that β_0 is measured in the local and β_0^g in the global coordinate system. The angles are defined in the mathematical positive direction of rotation (counterclockwise). Please note: for this figure the origin of the global coordinate system is chosen to coincide with X_0, which is also the origin of the local coordinate system. Of course, in general this is not the case.*

IMPLEMENTATION

It is evident why most practical problems are solved in an iterative way. Decomposing a problem into several terms of decreasing impact facilitates to solve it step by step, utilizing in each case the appropriate method. If the desired degree of accuracy is reached, remaining terms can be neglected. Of course, some problems might be too complex to be solved this way, but according to our current experience the CRS-attribute search seems to be none of that kind. Following the idea of step-by-step refinement, we chose an implementation that combines both methods of topography handling, reviewed in the last section, to a cascaded processing strategy. Doing this, most of the specific disadvantages of the single approaches can be compensated without loosing their individual benefits. Finally, a redatuming procedure provides a seamless transition to the tomographic inversion and other succeeding processing steps. A flowchart of this pragmatic strategy to handle topography within the CRS stack is depicted in Figure 4. In the following section, the individual steps of this flowchart will be discussed by means of a synthetic data example.

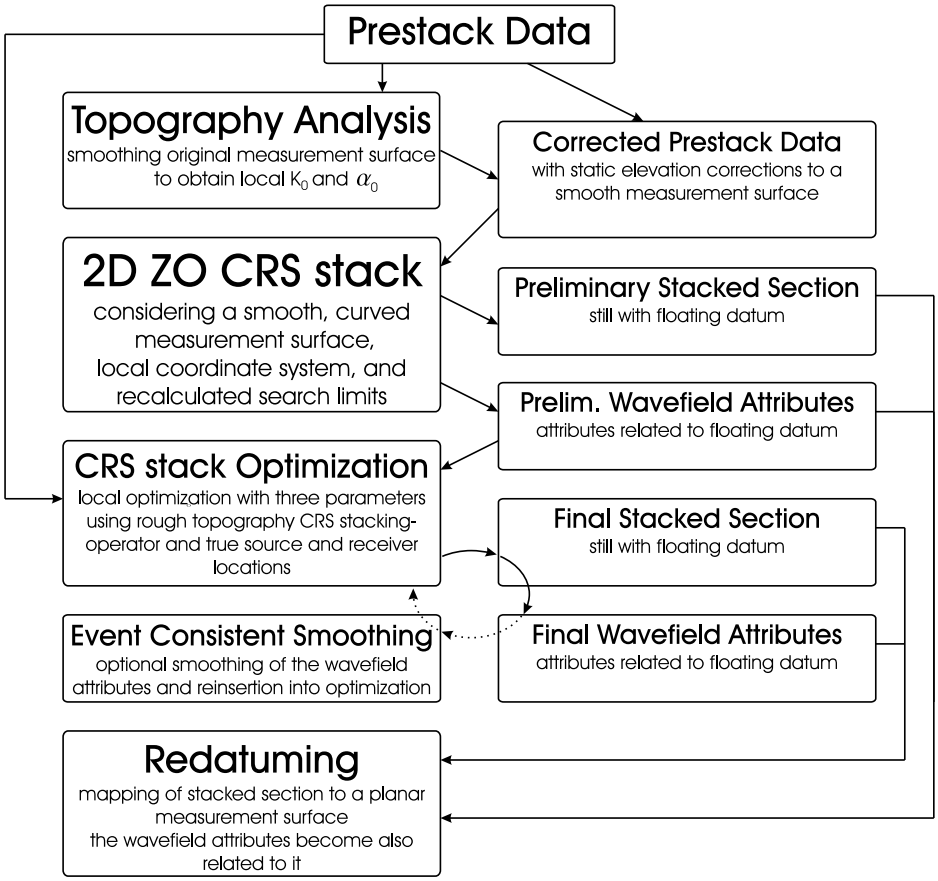

Figure 4: *Sketch of the extended CRS stack method for handling measurement surfaces with topography.*

SYNTHETIC DATA EXAMPLE

The synthetic data set used in this section to demonstrate the handling of topography within the CRS-stack-based imaging workflow was kindly provided by SAUDI ARAMCO. Figure 5 shows the underlying velocity model, simulating a situation which is very common in Arabian land-data acquisition. Looking at the measurement surface, depicted as a black line, a valley type structure with rapid changes in elevation can be observed. The subsurface structure consists of approximately twenty homogeneous layers, featuring about ten velocity inversions, although the interval velocities generally increase with depth.

The acquisition geometry of the prestack data is summarized in Table 1.

Context	Parameter	Value
Shot and receiver geometry	Number of shots	625
	Shot interval	16 m
	Maximum number of receivers	375
	Receiver interval	16 m
	Number of traces	199 593
Midpoint and offset geometry	Number of CMP bins	1250
	Maximum CMP fold	188
	Full offset range	-2992 . . . 2992 m
Recording parameters	Recording time	2 s
	Sampling interval	4 ms
	Mean frequency	30 Hz
	Maximum frequency	50 Hz

Table 1: *Information on the acquisition geometry of the prestack data.*

Initial CRS stack considering a smoothly curved measurement surface: In order to apply the CRS traveltime operator for a smoothly curved measurement surface [equation (7)] to our data set we have

1. to find an appropriate smooth reference surface,
2. to determine K_0 and α_0 for every X_0, and
3. to apply elevation static corrections that relate the prestack data to this surface.

For this purpose, it is necessary to consider that, in general, the larger the scale of the smoothing, the larger are the elevation static corrections which have to be applied. Nevertheless, the surface has to be smooth enough such that for every single stacking process the elevations of all contributing sources and receivers can be properly represented by a parabola. To control the scale of the smoothing a so-called smoothing aperture was introduced, which should, as a rule of thumb, be in the range of the maximum offset-aperture chosen for the wavefield attribute search and the stacking procedure.

In our recent implementation, steps 1 and 2 are performed by a module which fits, for every X_0, a circle to all source and receiver points located within the respective smoothing aperture. By these circles, the average dip, curvature and elevation is defined for every X_0 (Heilmann, 2002). To make the results stable and continuous along the line, this procedure is applied iteratively. A comparison between the original measurement surface and its smoothed counterpart can be found in Figure 6. The elevation-static correction time for every source and receiver location is calculated from the near-surface velocity and the differences in elevation of the true source and receiver points and their vertical projections onto the smoothed surface. This aims to simulate the traces as being recorded on the previously determined smooth measurement surface. For every ZO sample the kinematic wavefield attributes K_{NIP}, K_{N}, and β_0 are determined by means of three one-parameter searches. Thus, a specific (spatial) stacking operator [equation (7)] is defined for every sample of the ZO section. The summation process is performed in a user-defined aperture and/or in an aperture that accounts for the size of the projected first Fresnel zone. The latter can be estimated from the CRS attributes by comparing the approximated traveltime of the actual reflection event with the approximated traveltime of its associated diffraction event (characterized by the identity $K_{\mathrm{NIP}} = K_{\mathrm{N}}$). The locations where these events differ by half the temporal wavelet length define the extension of the projected first Fresnel zone and, thus, the optimum aperture to apply the attribute search and the stack.

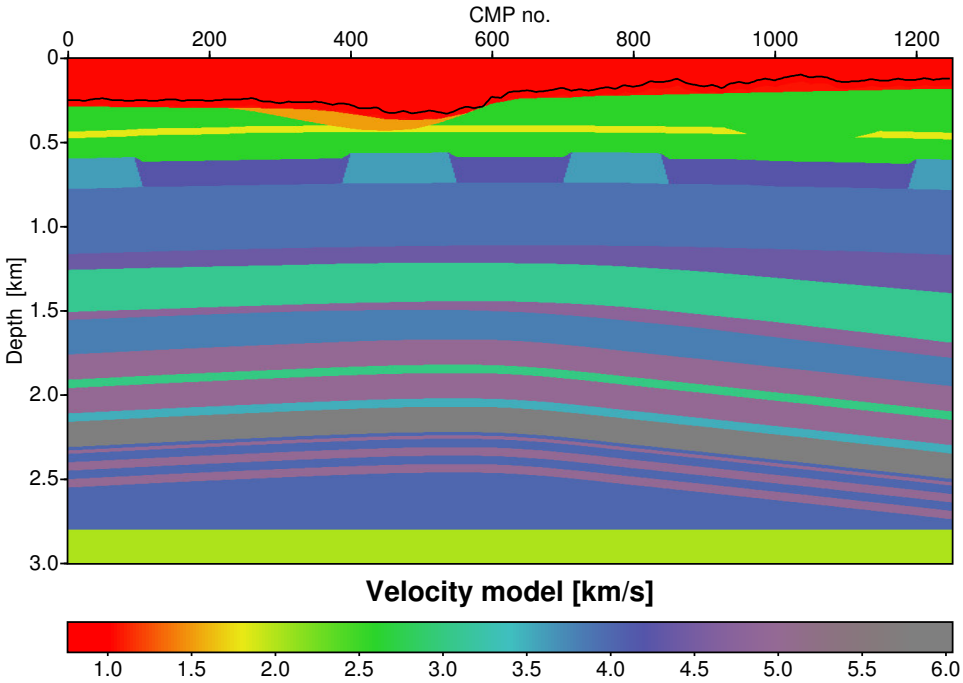

Figure 5: *Velocity model provided by* SAUDI ARAMCO*, which was used to generate the prestack data. The black line indicates the measurement surface.*

Event-consistent smoothing: At this stage, event-constent smoothing of the initial attributes (see, e.g., Mann and Duveneck, 2004) can be helpful to remove fluctuations and outliers. Since this process does not involve any loss of information about the parameterized reflection events—even in case of conflicting dip situations—it often provides significantly improved input for the subsequent optimization. However, for this synthetic example, where the high signal-to-noise ratio facilitates a very stable attribute search, the event-consistent smoothing of the initial CRS attributes had only a minor effect.

Three-parameter optimization considering the true topography: An important feature of the CRS traveltime operator for arbitrary topography [equation (1)] is that the emergence points of the ZO rays to be simulated can be chosen arbitrarily. This property provides the link to the initial results determined under the assumption of a smoothly curved measurement surface. Since the latter are related to an artificial smoothly curved measurement surface one has to choose this surface also as reference level for the optimization. By this means, the ZO rays to be simulated are identical in both cases. Therefore, it can be expected that the CRS attributes obtained in the previous step are close to their optimum values and, thus, well suited as initial values for a local three-parameter optimization using equation (1). For the latter, a simple and robust algorithm is used, i.e., the *flexible polyhedron search* according to Nelder and Mead (1965). In our case, where three parameters are searched-for, the polyhedron is a tetrahedron. The objective function is, as in case of the one-parameter searches, the semblance (Neidell and Taner, 1971), a measure for the coherence between the stacking operator and the (unknown) reflection response in the prestack data.
The simulated ZO section achieved by local optimization of the CRS attributes and subsequent stack is depicted in Figure 7. To confine the spatial extent of the stacking operator, the projected first Fresnel zone was taken into account. Both, the local optimization and the stacking itself were applied to the original, i.e., uncorrected, data using the CRS traveltime operator for arbitrary topography [equation (1)]. Consequently, any inaccuracies of the initial stack and especially of the initial attributes caused by the elevation statics should be compensated. Nevertheless, stack and attribute sections are still related to the floating datum corresponding to the smooth reference surface.

Redatuming: Floating datum sections are no appropriate input, neither for interpretation nor for further processing. Therefore, we implemented a redatuming procedure that relates the CRS stack results to a fictitious planar measurement surface above the smoothly curved reference level (see Figure 6). Due to the fact that the emergence angle of every simulated ZO ray is known, it is easy to forward-propagate them to a constant reference level—especially, if the velocity v_f between the smoothly curved and the planar surface is chosen to be equal v_0. In this case no refraction has to be considered when crossing the smoothly curved reference level. The mapping of the ZO samples of stack and attribute sections is composed of a lateral displacement Δx and a time shift Δt. Denoting the emergence point of the zero-offset ray at the planar reference level by $X'_0(x'_0, z'_0)$ the respective transformations read

$$x'_0 = x_0 + \Delta x = x_0 + (z'_0 - z_0)\,\tan\beta_0 \quad \text{and} \quad t'_0 = t_0 + \Delta t = t_0 + \frac{2\,(z'_0 - z_0)}{v_0\,\cos\beta_0}\,. \tag{9}$$

An important aspect to be considered by the redatuming procedure is that the stack amplitudes and especially the CRS attributes K_{NIP} and K_{N} alter their values while the ZO ray is forward-propagated upwards. The *propagation law* (see, e.g., Hubral and Krey, 1980) yields for the two wavefront radii K'_{NIP} and K'_{N} measured at the planar reference level

$$K'_{\mathrm{NIP}} = \left(\frac{1}{K_{\mathrm{NIP}}} + \frac{1}{2}\,\Delta t\,v_0\right)^{-1} \quad \text{and} \quad K'_{\mathrm{N}} = \left(\frac{1}{K_{\mathrm{N}}} + \frac{1}{2}\,\Delta t\,v_0\right)^{-1} \tag{10}$$

The values of the emergence angle are not altered by the redatuming, as no refraction occurs at the smoothly curved reference level. For mapping the stack amplitudes, the *geometrical spreading factor* calculated from the CRS attributes could be used to extrapolate appropriate values corresponding to the planar reference level. However, this is not yet implemented and the amplitudes are mapped without altering their values. The optimized CRS stack section after redatuming is depicted in Figure 8. For the sake of brevity, the redatumed sections of β_0, K_{NIP}, and K_{N} have been omitted. Instead of these sections, two sections of important properties directly deduced from the CRS attributes are shown.

In Figure 9, the normalized in-line geometrical spreading factor is displayed, calculated from the redatumed values of K_{NIP} and K_{N} according to the relation (see, e.g, Vieth, 2001)

$$|L_2| = \sqrt{\frac{2}{v_0}\,|K_{\mathrm{NIP}} - K_{\mathrm{N}}|^{-1}}\,. \tag{11}$$

The geometrical spreading has a major impact on the change in amplitude if transmission losses are negligible. If the geometrical spreading factor is applied to the zero-offset section, the resulting section displays the correct reflection coefficient for a seismic event if the source strength is considered. Such a true-amplitude section is of great advantage for geological interpretation, e.g., to find a hydrocarbon deposit. In 2-D, the amplitude is inverse proportional to the square root of the curvature of the propagating wavefront. Here, we did not account for the source strength, but used the normalized geometrical spreading factor as a natural gain function aiming to remove the influence of geometrical spreading from the stack section. The resulting stack section is displayed in Figure 10.

Figure 11 shows a NMO velocity section calculated from the optimized CRS attributes K_{NIP} and β_0 after redatuming according to the relation

$$v^2_{\mathrm{NMO}} = \frac{2v_0}{t_0\,\cos^2\beta_0\,K_{\mathrm{NIP}}}\,. \tag{12}$$

Please note that in order to display v_{NMO}, the signed square-root was used. Consequently, negative values in the display stand for imaginary NMO velocity values. The latter are caused by the lense like structure between CMP 400 and 600 that leads to caustics in the NIP wavefronts.

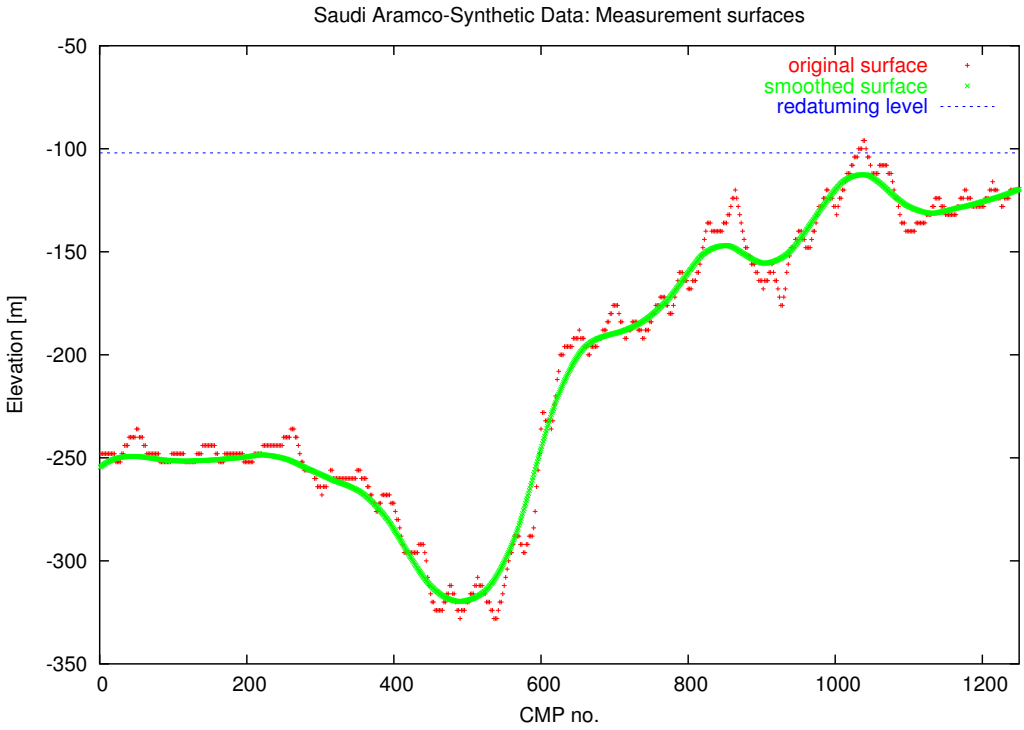

Figure 6: *Comparison between original and smoothed measurement surface. The planar measurement surface at $z = -102$ m used for the redatuming is also displayed.*

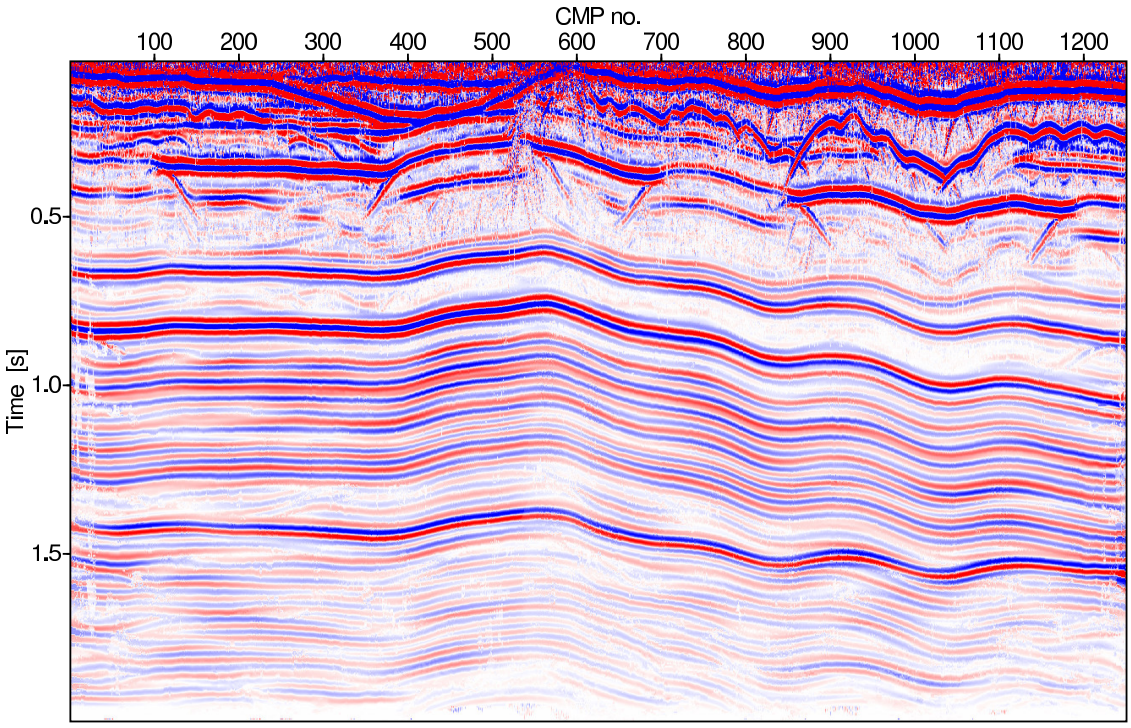

Figure 7: *Optimized CRS stack result for complex top-surface topography. The simulated zero-offset section is related to the smoothed measurement surface.*

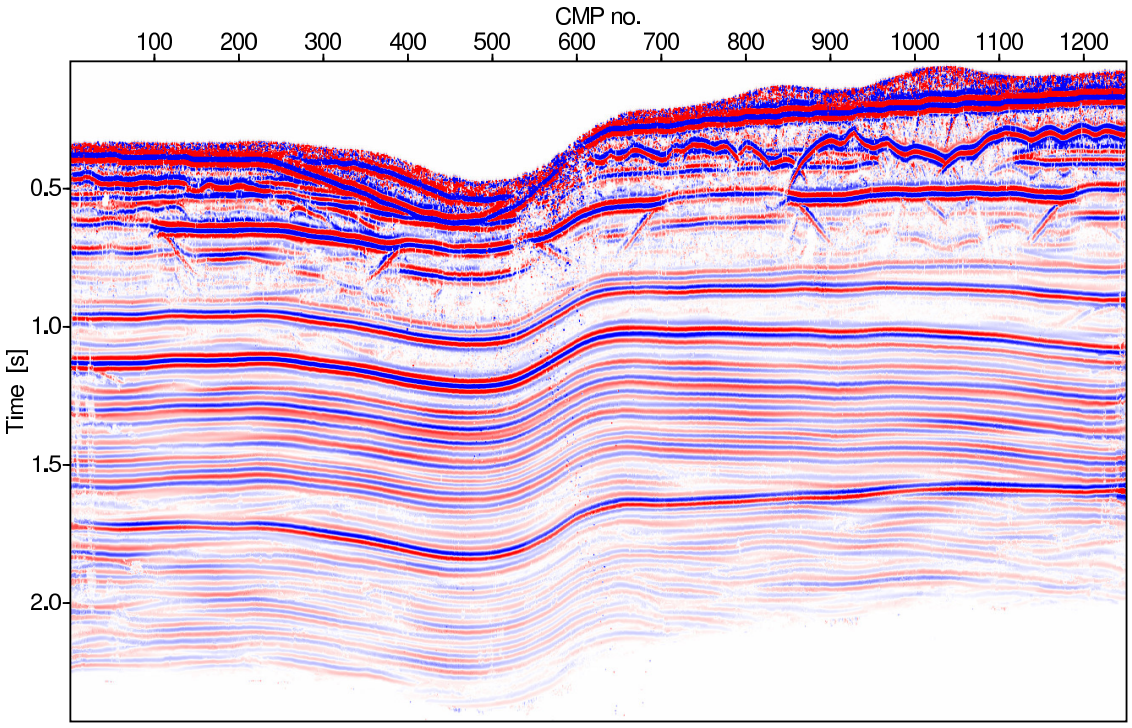

Figure 8: *Optimized CRS stack result after redatuming. The redatuming procedure relates the achieved results to a fictitious horizontal measurement surface at* $z = -102$ *m.*

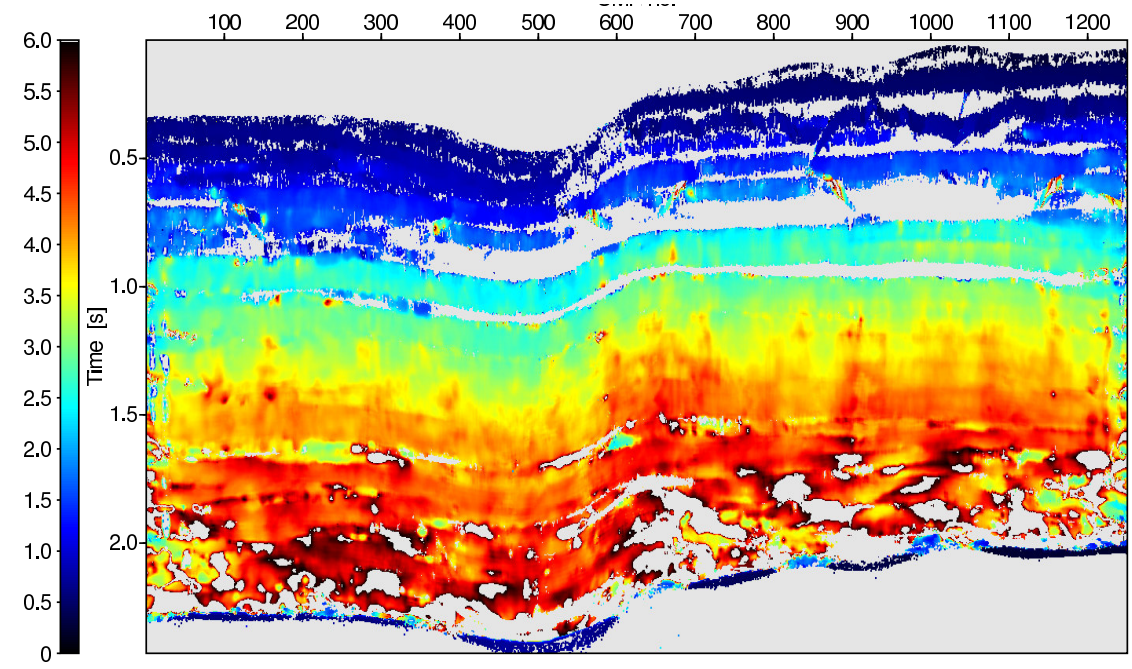

Figure 9: *Geometrical spreading factor calculated from optimized and smoothed CRS attributes. zero-offset samples with very low coherence value are masked out (grey), as they are not expected to be related to reliable attributes. This section is related to a fictitious horizontal measurement surface at* $z = -102$ *m.*

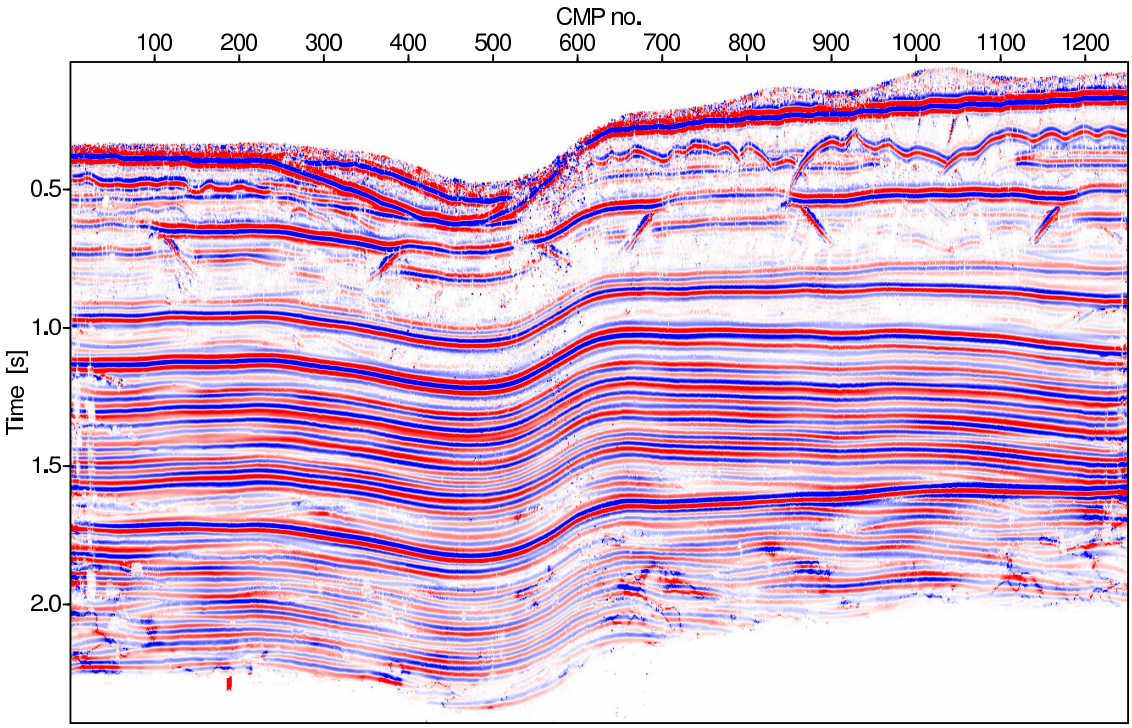

Figure 10: *Final CRS stack result after redatuming and amplitude correction with the geometrical spreading factor. The redatuming procedure relates the achieved results to a fictitious horizontal measurement surface at* $z = -102$ *m.*

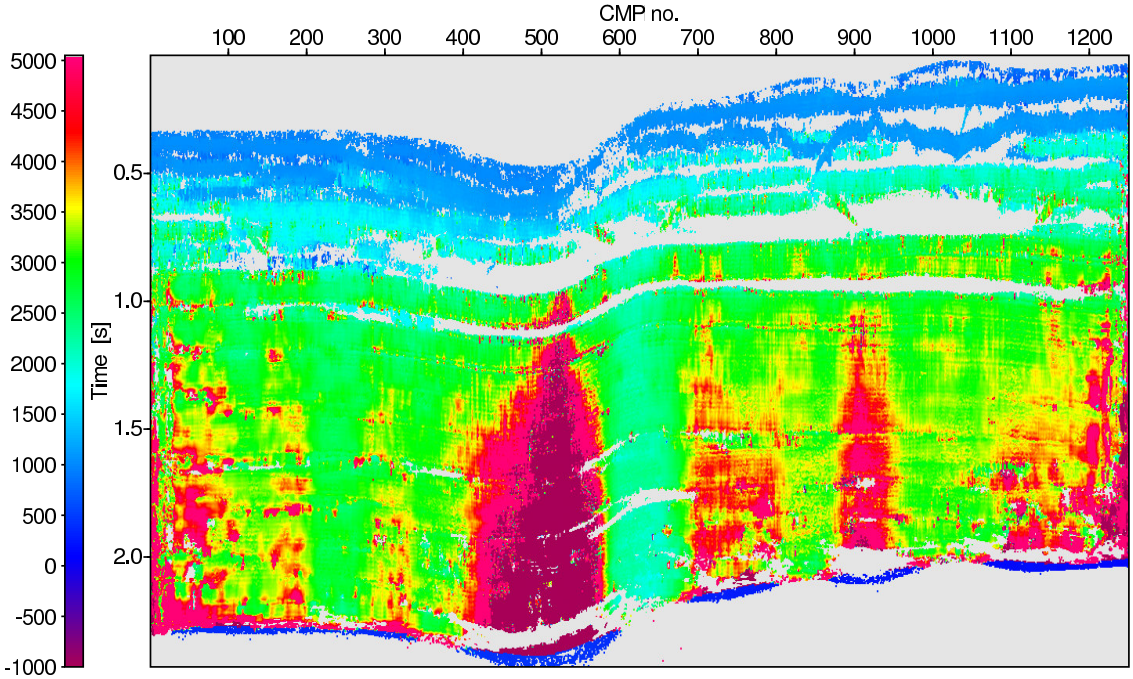

Figure 11: *Stacking velocity* v_{NMO} *[m/s] calculated from optimized CRS attributes. ZO samples with very low coherence value are masked out (grey), as they are not expected to be related to reliable attributes. A negative value actually indicates an imaginary value of* v_{NMO}*. This section is related to a fictitious horizontal measurement surface at* $z = -102$ *m.*

OUTLOOK & CONCLUSION

In this paper we presented a recent extention of the CRS-stack-based imaging workflow that is able to support arbitrary top-surface topography. A cascaded strategy for stacking and attribute extraction was introduced combining two different approaches of topography handling to a very efficient implementation. In a final step, the floating datum results of the CRS stack are mapped to a constant reference level above the actual topography, utilizing the previously extracted emergence angles. This redatuming procedure provides an ideal input for subsequent CRS-stack-based processing steps as the influence of the topography is fully removed. By means of a synthetic data example, the practical application of CRS stack and redatuming in case of rough top-surface topography was demonstrated. To enhance the obtained ZO section, the first projected Fresnel zone, calculated from the CRS attributes, was used as a natural gain function aiming to compensate for the influence of geometrical spreading. Results of subsequent processing steps as, e.g., tomographic inversion or poststack depth migration were not yet presented, but the authors are confident to show such results at this year's WIT meeting. First tests with PostSDM of the redatumed CRS stack results using the original velocity model showed promising results.

Currently, the presented implementation is also applied to a real data set. For this purpose, it is very important to consider a laterally variable near-surface velocity, since both, the static corrections of the initial search and the CRS stack operator used for the final optimization, strongly depend on this parameter. A topic of future research will be the implementation of CRS stacking operators for smoothly and arbitrarily curved topography that also account for a variable near-surface velocity gradient according to Heilmann (2002) and Chira and Hubral (2003).

ACKNOWLEDGMENTS

This work was kindly supported by the sponsors of the *Wave Inversion Technology (WIT) Consortium*, Karlsruhe, Germany. We gratefully acknowledge the permission of the Saudi Aramco Oil Co. to use and present their data.

REFERENCES

Červený, V. (2001). *Seismic Ray Theory*. Cambridge Univ. Press, New York, 2001 (ISBN 0-521-36671-2).

Chira, P. and Hubral, P. (2003). Traveltime formulas of near-zero-offset primary reflections for curved 2D measurement surface. *Geophysics*, 68(1):255–261.

Chira, P., Tygel, M., Zhang, Y., and Hubral, P. (2001). Analytic CRS stack formula for a 2D curved measurement surface and finite-offset reflections. *Journal of Seismic Exploration*, 10(1-3):245–262.

Heilmann, Z. (2002). The Common-Reflection-Surface Stack under Consideration of the Acquisition Surface Topography and of the Near-Surface Velocity Gradient. Master's thesis, Karlsruhe University, http://www-gpi.physik.uni-karlsruhe.de/pub/wit/Downloads/diplthesis-zheilmann.pdf.

Heilmann, Z. (2003). Extensions of the Common-Reflection-Surface Stack Considering the Surface Topography and the Near-Surface Velocity Gradient. In *Ext. Abstr., 8th International Congress, Soc. Bras. Geofísica (SBGf), Rio de Janeiro*.

Höcht, G. (1998). Common-Reflection-Surface stack. Master's thesis, Karlsruhe University.

Hubral, P. (1983). Computing true amplitude reflections in a laterally inhomogeneous earth. *Geophysics*, 48(8):1051–1062.

Hubral, P., editor (1999). *Special Issue on Macro-Model Independent Seismic Reflection Imaging*, volume 42(3,4) of *Journal of Applied Geophysics*, Amsterdam. Elsevier.

Hubral, P. and Krey, T. (1980). *Interval velocities from seismic reflection traveltime measurements*. Soc. Expl. Geophys.

Jäger, R., Mann, J., Höcht, G., and Hubral, P. (2001). Common-reflection-surface stack: Image and attributes. *Geophysics*, 66:97–109.

Mann, J. (2002). *Extensions and applications of the Common-Reflection-Surface stack method*. Logos Verlag, Berlin.

Mann, J. and Duveneck, E. (2004). Event-consistent smoothing in generalized high-density velocity analysis. In *Extended Abstracts,*, Session: ST1.1. 74th Annual Internat. Mtg., Soc. Expl. Geophys.

Müller, T. (1999). *The Common-Reflection-Surface stack method - seismic imaging without explicit knowledge of the velocity model*. Der andere Verlag, Bad Iburg.

Neidell, N. S. and Taner, M. T. (1971). Semblance and other coherency measures for multichannel data. *Geophysics*, 36(3):482–497.

Nelder, J. A. and Mead, R. (1965). A simplex method for function minimization. *Computer Journal*, 7:308–313.

Vieth, K.-U. (2001). *Kinematic wavefield attributes in seismic imaging*. PhD thesis, Karlsruhe University, http://www.ubka.uni-karlsruhe.de/vvv/2001/physik/2/2.pdf.

von Steht, M. (2004). The Common-Reflection-Surface Stack under Consideration of the Acquisition Surface Topography – Combined Approach and Data Examples. Master's thesis, Karlsruhe University, http://www-gpi.physik.uni-karlsruhe.de/pub/wit/Downloads/diplthesis-mvsteht.pdf.

Zhang, Y. (2003). *Common-Reflection-Surface Stack and the Handling of Top Surface Topography*. Logos Verlag, Berlin.

Zhang, Y. and Wu, R. (2004). CRS stack and redatuming for rugged surface topography: a synthetic data example. In *Ext. Abstr., 74th Annual Internat. Mtg., Soc. Expl. Geophys.*, Session: SP4.6.